1568. Numerical and experimental investigation of aerodynamic noise from automotive cooling fan module

Maotao Zhu[1], Kuan Wang[2], Pengfei Zhang[3], Zhijun Li[4]

[1, 2, 3]School of Automotive and Traffic Engineering, Jiangsu University, Jiangsu, China
[4]Jiangsu Chaoli Electric Co., Ltd., Jiangsu, China
[2]Corresponding author
E-mail: [1]*zhumt@ujs.edu.cn*, [2]*wk_vip@126.com*, [3]*shicunzhijian8@126.com*, [4]*lizhijun605@126.com*

Abstract. The numerical investigation of automotive cooling fan module aerodynamic noise based on Computational Fluid Dynamics (CFD) / Computational Aero Acoustics (CAA) hybrid method is taken. Considering the influence of fan shroud, an aerodynamic steady simulation is made at first, and then Large Eddy Simulation (LES) with the Smagorinsky model is applied to capture the unsteady pressure data on fan surface. Based on Lowson formula, a prediction of aerodynamic noise is made by Boundary Element Method (BEM). Finally, the prediction results are compared with the experimental results, which show that the acoustic response is with a strong dipole character. Sound pressure level (SPL) at receive points increased with air flow rate. SPL at outlet was higher than inlet. Tonal noise was the major component of the aerodynamic noise. Broadband noise was relatively lower and distributed evenly. Predicted results is consistent with the experimental results, which validates the numerical prediction method. This method can provide a reference to acoustic optimization.

Keywords: cooling fan module, aerodynamic noise, CFD, CAA, hybrid approach.

1. Introduction

Noise reduction requirement has been increased with the increasing number of automotive in recent years. Cooling fan module is not only an important component of cooling system, but also is the main noise source of the automotive. It is necessary to reduce automotive cooling fan noise [1]. Cooling fan module noise includes aerodynamic noise, vibration noise and electromagnetic noise, among which the aerodynamic noise dominates. Therefore, the reduction of aerodynamic noise of the cooling fan module is essential to the automotive Noise Vibration and Harshness (NVH) performance.

Traditional method of automotive cooling fan design mainly depends on trial-and-error method, which is very costly. Nowadays with the rapid development of Computational Fluid Dynamics (CFD) and Computational Aero Acoustics (CAA) technology, numerical prediction of aerodynamic noise has become increasingly achievable. Maaloum made an aeroacoustic performance evaluation of axial flow fans based on the unsteady pressure field on the blade surface [2]. Suzuki studied on the fan noise reduction for automotive radiator cooling fans [3]. Carolus predicted axial flow fan broad-band noise using LES [4]. Nashimoto detected the aerodynamic noise sources over a rotating radiator fan blade for automobile [5]. Udawant predicted fan noise using CFD and made its validation [6]. Lee developed low-noise cooling fan using uneven fan blade spacing [7]. Khelladi predicted tonal noise from a high rotational speed centrifugal fan [8]. Krishna reduced the motor fan noise using CFD and CAA simulations [9]. Udawant designed and developed a radiator fan for automotive application [10]. Tannoury studied the influence of blade compactness and segmentation strategy on tonal noise prediction of an automotive engine cooling fan [11]. Gérard made the use of a beat effect for the automatic positioning of flow obstructions to control tonal fan noise by theory and experiments [12]. Ota developed a high efficient radiator cooling fan for automotive application [13]. Becher investigated of the applicability of numerical noise prediction of an axial vehicle cooling fan [14]. Zanon made a numerical investigation of location and coherence of broadband noise sources for a low speed axial HVAC Fan [15]. However, most previous studies only concerned the fan itself but ignored the fan shroud. Under

actual condition, the fan and fan shroud are interacted with each other. The impact of fan shroud for the flow field and sound field needs to be studied.

In this study the automotive cooling fan module is taken as the study object. CFD and CAA hybrid method is applied to predict aerodynamic noise from the module. Considering the impact of fan shroud for flow field, the transient simulation is carried out to capture the noise source information by the LES with the Smagorinsky model. Then taking the impact of fan shroud for sound propagation into consideration, the acoustic model is set up by BEM to predict the aerodynamic noise. Finally, the noise experiment is made to verify the accuracy of the aerodynamic numerical prediction.

2. Aerodynamic simulation

2.1. Theoretical method

The key technique of large-eddy simulation is the separation between large and small scales. The governing equations for LES are obtained by filtering the time-dependent Navier-Stokes equations in the physical space. The filtering process effectively filters out eddies whose scales are smaller than the filter width or grid spacing used in the computations. The resulting equations thus govern the dynamics of the large eddies [4].

A filtered variable is denoted in the following by an overbar and is defined by:

$$\bar{\Phi}(\boldsymbol{x}, t) = \int_D \Phi(\boldsymbol{x}', t) G(\boldsymbol{x} - \boldsymbol{x}') d\boldsymbol{x}', \tag{1}$$

where $\boldsymbol{x}$ is one fluid particle coordinate in the fluid domain, $\boldsymbol{x}'$ is another fluid particle coordinate in the fluid domain, D is the fluid domain, and G is the filter function that determines the scale of the resolved eddies:

$$\bar{\Phi}(\boldsymbol{x}, t) = \frac{1}{V} \int_V \Phi(\boldsymbol{x}', t) d\boldsymbol{x}', \quad \boldsymbol{x}' \in V, \tag{2}$$

where V is the control volume. The filter function $G(\boldsymbol{x} - \boldsymbol{x}')$ implied here is then:

$$G(\boldsymbol{x} - \boldsymbol{x}') = \begin{cases} \dfrac{1}{V}, & \boldsymbol{x}' \in V, \\ 0, & \boldsymbol{x}' \notin V. \end{cases} \tag{3}$$

Filtering the Navier-Stokes equations leads to additional unknown quantities. In the following the theory will be outlined for the incompressible equations. The filtered incompressible momentum equation can be written in the following way:

$$\frac{\partial \bar{U}_i}{\partial t} + \frac{\partial}{\partial x_j}(\bar{U}_i \bar{U}_j) = -\frac{1}{\rho}\frac{\partial \bar{p}}{\partial x_i} + \frac{\partial}{\partial x_j}\left[v\left(\frac{\partial \bar{U}_i}{\partial x_j} + \frac{\partial \bar{U}_j}{\partial x_i}\right)\right] - \frac{\partial \tau_{ij}}{\partial \tau_j}, \tag{4}$$

where i and j are two orthogonal directions. τ_{ij} denotes the subgrid-scale stress. It includes the effect of the small scales and is defined by:

$$\tau_{ij} = \overline{U_i U_j} - \bar{U}_i \bar{U}_j. \tag{5}$$

The large scale turbulent flow is solved directly and the influence of the small scales is taken into account by appropriate subgrid-scale (SGS) models. An eddy viscosity approach is used that relates the subgrid-scale stresses τ_{ij} to the large-scale strain rate tensor $\bar{S}_{ij}$ in the following way:

$$-\left(\tau_{ij} - \frac{\delta_{ij}}{3}\tau_{kk}\right) = 2v_{sgs}\bar{S}_{ij}, \quad \bar{S}_{ij} = \frac{1}{2}\left(\frac{\partial \bar{U}_i}{\partial x_j} + \frac{\partial \bar{U}_j}{\partial x_i}\right), \tag{6}$$

where the eddy viscosity v_{sgs} represents all turbulent scales, the subgrid-scale viscosity only represents the small scales. In this study, the sub-grid scale velocity fluctuations are modeled with a dynamic Smagorinsky model. The schematic geometrical model for Eqs. (1)-(6) can be referred in [16].

2.2. Aerodynamic modeling

The reasonable aerodynamic model is the important foundation of numerical aeroacoustic prediction. The investigated model is a single 7-blade automotive cooling fan module which is presented in Fig. 1(a). The fan flow field is mainly affected by the blade and the shroud frame, therefore some details are simplified and the simplified fan module is shown in Fig. 1(b).
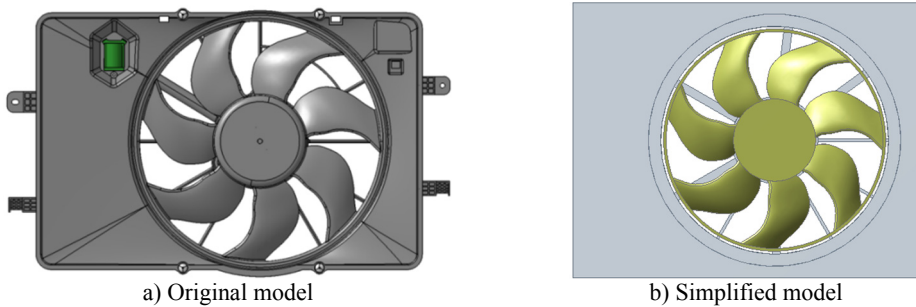

a) Original model b) Simplified model

Fig. 1. Cooling fan module model

The aerodynamic model is shown in Fig. 2(a). Rotating domain and stationary domain are established in the CFX 15.0. According to the noise experiment environment, the total length of the external stationary domain 2000 mm. Inlet and outlet are on the front and back sides of the external stationary domain.
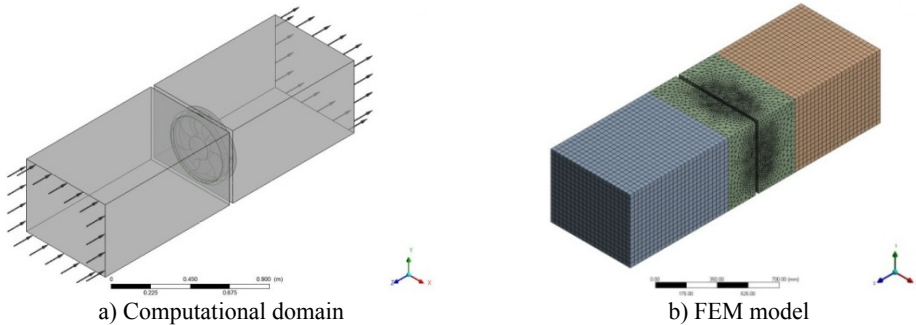

a) Computational domain b) FEM model

Fig. 2. Aerodynamic model

The FEM model is shown in Fig. 2(b), which is generated in ICEM CFD 15.0. Considering the complexity of the blade surface, hexahedral inflation layer grids with fine resolution are created near the surface of blades for the accuracy of capturing the pressure fluctuations. Pyramid and tetrahedral grids are used in the rest area of rotational domain. And in the middle part of stationary domain, tetrahedral grids are generated for improving the computational efficiency. Hexahedral grids are created in the front and rear parts of stationary domain, whose geometry are relatively simple, to increase both computational accuracy and efficiency. The number of elements and nodes are given in the Table 1.

The flow field is composed of rotational domain and stationary domain, so the interface between two domains should be considered. The interfaces of two domains are set as "Frozen Rotor" in steady computation and "Transient Rotor Stator" or called as "Sliding mesh method" is set in unsteady computation to capture the transient relative motions between rotors and stators. In this approach, the interface position is updated each physical time step and the flow variables on the interfaces are transferred to each other through the meshes of the interfaces.

The inlet boundary condition is defined as "static pressure condition" as 0 Pa to represent the ambient pressure and the outlet boundary condition is defined as "static pressure condition" as 0 Pa as well. The wall condition is defined as "adiabatic, no slip condition". Because the flow Mach number is below 0.2, the gas is defined as non-compressible gas. 3 cases are set to capture the aerodynamic noise source information in 3 different operating conditions. The case setting is shown in Table 2.

Table 1. Mesh information

Element domain	Number of elements	Number of nodes
Rotating domain	171,7771	52,0422
Stationary domain	192,3511	64,1171
Total	364,1282	116,1593

Table 2. Case setting

Case	Operating Volt (V)	Rotation Speed (RPM)
1	12.0	1900
2	13.0	2000
3	13.5	2100

The unsteady computation is based on the steady state flow field result. The cut-off frequency is set as 2500 Hz, so according to Nyquist sampling theorem the sampling interval is set as 0.0002 s. The maximum number of timesteps is set as 10,000. In order to ensure the convergence of flow field computation, the monitors of coefficient loop convergences are set up, including pressure and velocity at the both inlet and outlet.

2.3. Results and discussion

Fig. 3 and Fig. 4 show the fluctuating pressure field on the pressure and the suction side of fan and shroud in Case 3. The pressure of suction side is negative but the pressure near the blade leading edge is positive. The turbulent flow on the pressure side presents more significant fluctuations than those observed on the suction side. In addition, there are more significant interaction in the areas close to the trailing edge than the leading edge of the blades. The aerodynamic noise is mainly generated by the interaction between the flow and the leading edges. The pressure field on the shroud surface is very inhomogeneous, which demonstrates the shroud affects the air distribution behind the fan blade surface significantly. The interaction between the fan and the shroud leads to pressure fluctuation and vortex disturbance, which are the major aerodynamic noise sources areas.

Fig. 5 and Fig. 6 depict the turbulence kinetic energy and turbulence eddy frequency distributions on the cross-sectional plane near the fan blades and the stability bars in Case 3. It is acknowledged that the turbulent kinetic energy and turbulence eddy frequency are representations of the magnitude of broadband noise sources [8]. Interestingly, the turbulence kinetic energy and turbulence eddy frequency distributions have similar patterns, which reach the maximum near the tailing edges and the inside of the ring. These intense contours may be a result of the fierce interaction of the air in the blade passage with the flow through shroud. According to the vortex sound theory, these eddies make great contributions to the aerodynamic noise generation.
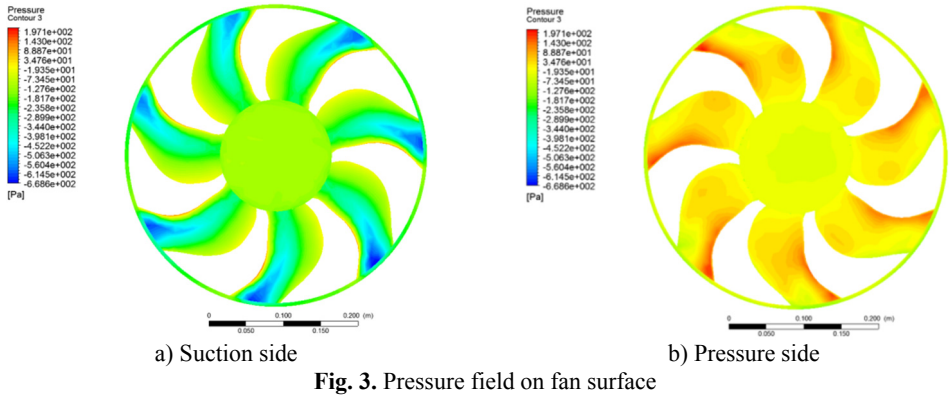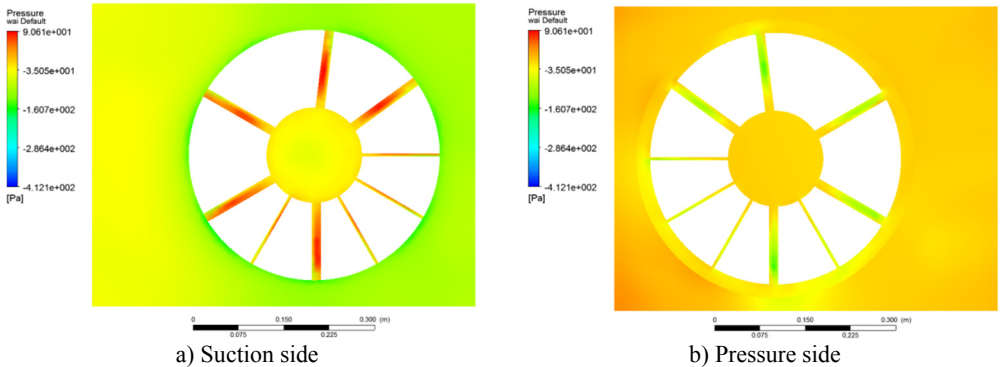
a) Suction side   b) Pressure side

Fig. 3. Pressure field on fan surface

a) Suction side   b) Pressure side

Fig. 4. Pressure field on shroud surface

a) Near the fan blades   b) Near the stability bars
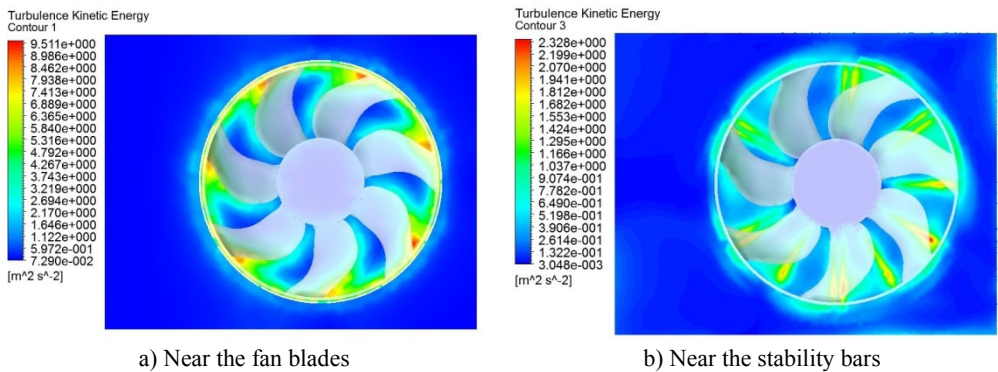
Fig. 5. Turbulence kinetic energy

3. Aeroacoustic simulation

3.1. Theoretical method

The aeroacoustic analogy allows to find an expression for the incident acoustic field generated by a rotating fan at the blade passing frequency and harmonics. Some assumptions are taken into account to develop Lowson formula [17]: the fluid is incompressible, the flow is subsonic with a low Mach and high Reynolds numbers and the point O defining the observer is located in a distance supposed very large in front of that defining the source S, which is shown in Fig. 7. When stator is at the outlet, axial and tangential contributions of the radiated pressure at frequency $mB\Omega$:

$$p_{in\,c}^{mB}(x) = \frac{-imB^2\Omega e^{-\frac{imB\Omega R}{c_0}}}{4\pi c_0 R} \sum_{s=-\infty}^{\infty} F_{mB} e^{-i(mB+sV)\left(\varphi+\frac{\pi}{2}-\alpha_0\right)},$$

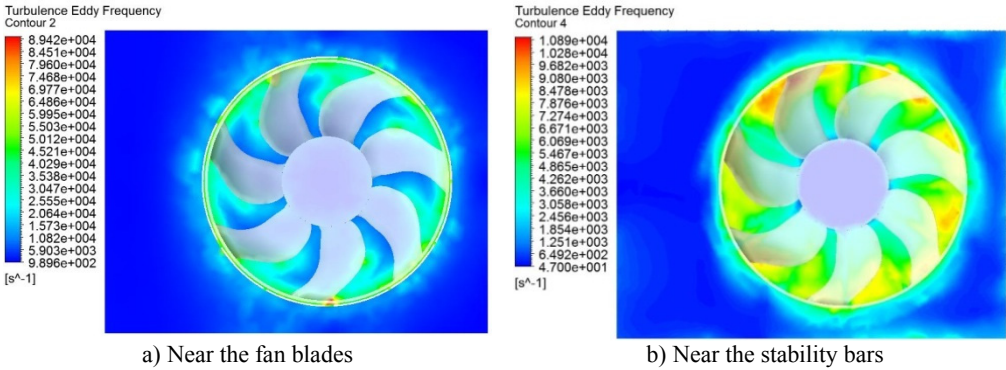$$J_{mB+sV}(-mBM\sin\theta) \cdot \left[\cos\gamma'^{\cos\theta} - \frac{mB+sV}{mBM}\sin\gamma'\right].$$

(7)

Turbulence Eddy Frequency
Contour 2
8.942e+004
8.451e+004
7.960e+004
7.468e+004
6.977e+004
6.486e+004
5.995e+004
5.503e+004
5.012e+004
4.521e+004
4.029e+004
3.538e+004
3.047e+004
2.555e+004
2.064e+004
1.573e+004
1.082e+004
5.903e+003
9.896e+002
[s^-1]

Turbulence Eddy Frequency
Contour 4
1.089e+004
1.028e+004
9.682e+003
9.080e+003
8.478e+003
7.876e+003
7.274e+003
6.671e+003
6.069e+003
5.467e+003
4.865e+003
4.262e+003
3.660e+003
3.058e+003
2.456e+003
1.854e+003
1.251e+003
6.492e+002
4.700e+001
[s^-1]

a) Near the fan blades   b) Near the stability bars

Fig. 6. Turbulence eddy frequency

Radial contribution:

$$p_{in\,c}^{mB}(\mathbf{x}) = \frac{mB^2\Omega e^{-\frac{imB\Omega R}{c_0}}}{4\pi c_0 R} \sin\theta \sum_{s=-\infty}^{\infty} F_{mB} e^{-i(mB+sV)\left(\varphi+\frac{\pi}{2}\right)},$$

$$J'_{mB+sV}(-mBM\sin\theta),$$

(8)

where m is the harmonic number, B is the number of rotor blades, Ω is the rotation speed, R is the distance from the observer, c_0 is the speed of sound, F_{mB} is the Fourier series of the total force on a compact blade segment, M is the rotational Mach number, θ, φ and γ are defined in Fig. 7, V is the number of stator vanes. α_0 is the phase angle.

The pressure field is captured from the loading force on a reference rotor blade or a reference stator vane. The force can be computed from the pressure fluctuations in time domain obtained from previous CFD unsteady computation. The resulting loading force is applied at one point of the blade. The representation of the fan by a single fan source is a good approximation when the size of the blades is small compared to the wavelength. When the size of the blade is very large and the fan cannot be considered as a compact source, the blade can be subdivided in a set of segments where each segment can be replaced by an equivalent source.
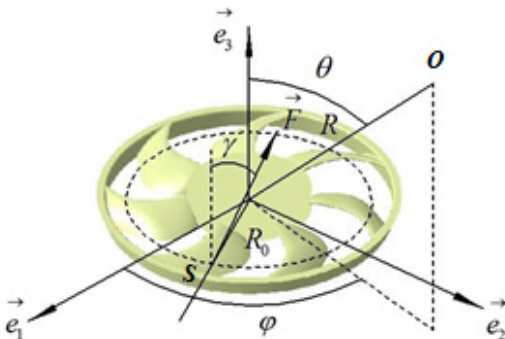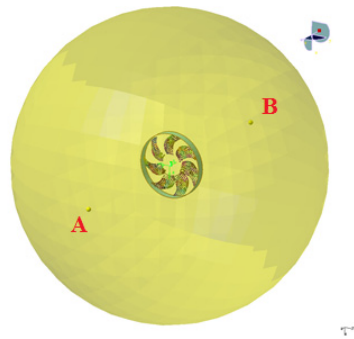

Fig. 7. Reference of the fan   **Fig. 8.** Acoustic model

3.2. Aeroacoustic modeling

The acoustic model is established in the commercial program LMS Virtual. Lab 13.1. Considering the impact of shroud to the noise propagation, acoustic boundary element mesh is established by Boundary Element Method, where the sound pressure is represented on the boundary elements. Fig. 8 depicts the boundary element mesh of the domain, where a cylinder field point mesh is created to represent the shroud and a spherical field point mesh ($R = 1$ m) is established around the fan as the acoustic response field. In addition, two receiving points are set at inlet that 1 m before the fan center as point A and at outlet 1 m behind the fan center as point B along the rotation axis.

Fan blade surface pressure fluctuation data are imported and the acoustic fan source equivalence is created. Fan can be modelled as a cloud of rotating point dipoles in the acoustic model. With the new feature in LMS Virtual. Lab 13.1, automatic detection of blades and generation of segments (point dipoles) are accessible. In this study the maximum analysis frequency is set as 2500 Hz so that one blade is equivalent to 11 point rotating dipoles automatically. Because the size of the blades is small compared to the wavelength, it is reasonable in both simulation accuracy and efficiency. As a result the entire fan is represented by 77 point rotating dipoles as aeroacousitc sources.

3.3. Results and discussion

The blade forces are visualized for the verification of their consistency. The variations of the axial force fluctuation over the blades over 0.06 s in 3 cases are presented in Fig. 9. 13, 14 and 15 peaks corresponding to the 7 fan blades occur over 0.06 s in Case 1, Case 2 and Case 3. With the increase of rotation speed, the force fluctuation both in average amplitude and in terms of fluctuation is also increasing. In addition, the most significant force fluctuation appears in Case 3. It is so logical for an axial fan that the radial and tangential components of the forces are negligible compared to axial component.
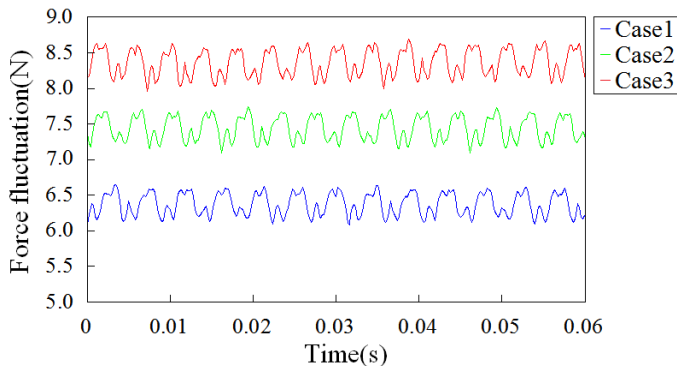

Fig. 9. Axial force fluctuation over fan blades vs. time in 3 cases

The two-dimensional sphere sound pressure distributions of Case 3 from 1×Blade Passing Frequency (BPF) to 3×BPF are shown in Fig. 10. The axial dipole characteristic at 1×BPF to 2×BPF are obvious and sound power is more concentrated. 3×BPF sound field still demonstrates dipole characteristic, but the axial deflection occurs.

Tonal noise and broadband noise are computed in the time domain and by the Fourier transform the SPL spectrums are predicted. Fig. 11 demonstrates the predicted SPL spectrums in 3 cases at two receiving points. As can be seen the SPL under 500 Hz is low while fluctuating around 30 dB after 500 Hz. There are obvious noise peaks at 1×BPF to 9×BPF, and at 2×BPF the maximum peak occurs. Tonal noise is higher than broadband noise, which shows tonal noise

occupies the major part of the aerodynamic noise at high rotation speed. At the same receiving point, tonal noise and broadband noise increases with rotation speed.
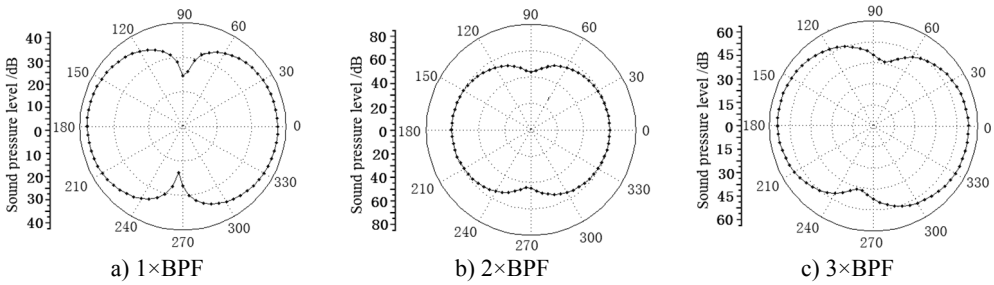

a) 1×BPF

b) 2×BPF

c) 3×BPF

Fig. 10. Predicted sound pressure distribution at different BPF
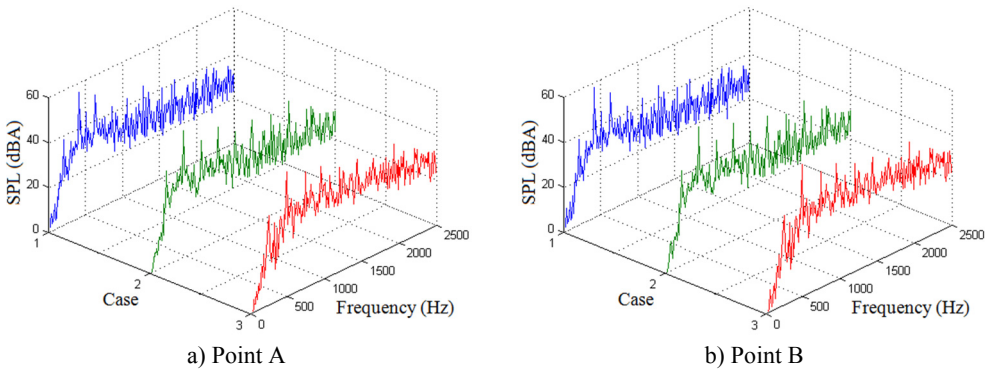

a) Point A

b) Point B

Fig. 11. Predicted SPL spectrums at two receiving points

For the verification of the noise prediction of the cooling fan module, the noise experiment of the cooling fan module is carried out in the semi-anechoic chamber. The semi-anechoic chamber is 4.0 m×3.5 m×3.8 m and the environmental noise is below 20 dB (A). Noise experiment equipment is shown in Fig. 12. B&K 3560 multichannel analyzer and two microphones are used in the experiment. The microphone A and B are 1 m over the ground and the positions are as same as receiving point A and B in the simulation, which are demonstrated in Fig. 13.
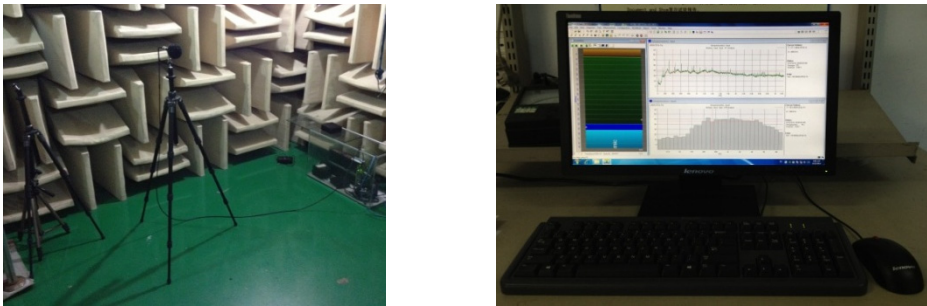

Fig. 12. Noise experiment equipment

Fig. 14 demonstrates experimental SPL spectrum results in 3 cases at two receiving points. As can be seen in all cases, the SPL of tonal noise prediction and experimental results agree well. There are larger fluctuations in broadband noise prediction results than experimental results, but the trend remains in good agreement with the experimental values, which verifies the accuracy of the numerical prediction of aerodynamic noise.
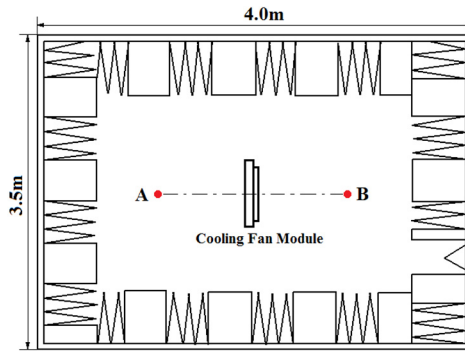
Fig. 13. Top view of the noise experiment environment

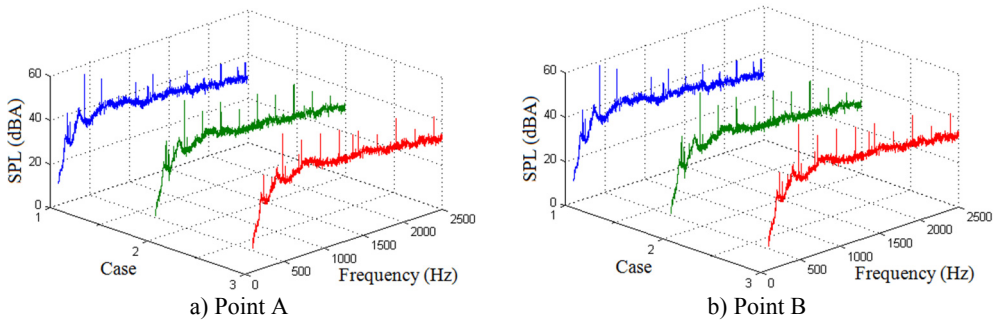a) Point A   b) Point B

Fig. 14. Experimental SPL spectrums at two receiving points

Fig. 15 is a comparison of the predicted results and the experimental results of the sound pressure level at two receiving points. Inlet and outlet sound pressure levels increase with increasing flow rate, and SPL in Case 3 is maximized. SPL at the export is larger than the import, which demonstrates that the impact of the dipole source to outlet is larger than inlet. SPL simulation results are smaller than the experimental results and the average relative error is less than 5 %. Part of these differences between the experimental and the predicted results can be attributed to the following reasons. On one hand, the fan blades are set as the only sources of the aerodynamic noise while the shroud frame noise, which is considered as stator noise, is neglected. On another, only aerodynamics noise is taken into account in the simulation. However, the experiment results contain aerodynamics noise and other noises, such as the vibration noise and electromagnetic noise from the electromotor of cooling fan module. Therefore in the next step of aeroacoustic simulation, both the stator noise and flow-introduced vibration noise should be taken into consideration to make the prediction results more accurate.
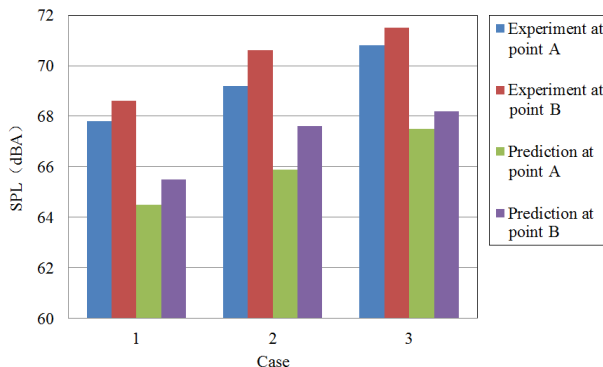

Fig. 15. SPL comparisons between the experiment and prediction at two receiving points

4. Conclusion

A complete cooling fan module CFD model is established using Large Eddy Simulation (LES) to capture the fan sound source information in three cases. Considering the impact of fan shroud for sound propagation, a boundary element method (BEM) model is set up for cooling fan module aerodynamic noise prediction. Finally experimental verification is taken. Conclusions are as follows: (1) Fan shroud impediment to air flow makes the blade surface pressure fluctuations increasing so that the aerodynamic noise increases. (2) The sound field is with strong axial dipole characteristic at low frequencies while axial deflection occurs at high frequencies. (3) Tonal noise is major part of the aerodynamic noise at high rotation speed. (4) At the same receiving point, tonal noise and broadband noise increase with the rotation speed. (5) The aerodynamic noise prediction is accurate, which can provide a reference for low-noise design.

Acknowledgements

References

[1] **Yoshida K., Semura J., Kohri I., Kato Y.** Reduction of the BPF noise radiated from an engine cooling fan. SAE Technical Paper, 2014.
[2] **Maaloum A., Kouidri S., Rey R.** Aeroacoustic performance evaluation of axial flow fans based on the unsteady pressure field on the blade surface. Applied Acoustics, Vol. 65, 2004, p. 367-384.
[3] **Suzuki A., Soya A.** Study on the fan noise reduction for automotive radiator cooling fans. SAE Technical Paper, 2005.
[4] **Thomas Carolus, Marc Schneider, Hauke Reese** Axial flow fan broad-band noise and prediction. Journal of Sound and Vibration, Vol. 300, 2007, p. 50-70.
[5] **Nashimoto A., Akuto T., Nagase Y., Yoda T., et al.** Detection of aerodynamic noise sources over a rotating radiator fan blade for automobile. SAE Technical Paper, 2007.
[6] **Udawant K., Tandon V., Raju S., Chugh K., et al.** Fan noise prediction using CFD and its validation. SAE Technical Paper, 2007.
[7] **Lee J., Nam K.** Development of low-noise cooling fan using uneven fan blade spacing. SAE Technical Paper, 2008.
[8] **Khelladi S., Kouidri S., Bakir F., Rey R.** Predicting tonal noise from a high rotational speed centrifugal fan. Journal of Sound and Vibration, Vol. 313, 2008, p. 113-133.
[9] **Rama Krishna S., Rama Krishna A., Ramji K.** Reduction of motor fan noise using CFD and CAA simulations. Applied Acoustics, Vol. 72, 2011, p. 982-992.
[10] **Udawant K., Tandon V., Joshi A., Srinivasan M.** Design and development of radiator fan for automotive application. SAE Technical Paper, 2012.
[11] **Tannoury E., Khelladi S., Demory B., et al.** Influence of blade compactness and segmentation strategy on tonal noise prediction of an automotive engine cooling fan. Applied Acoustics, Vol. 74, 2013, p. 782-787.
[12] **Gérard A., Berry A., Masson P., Moreau S.** Use of a beat effect for the automatic positioning of flow obstructions to control tonal fan noise: theory and experiments. Journal of Sound and Vibration, Vol. 332, 2013, p. 4450-4460.
[13] **Ota H., Yuichi K., Yukio O., Hiroshi Y.** Development of high efficient radiator cooling fan for automotive application. SAE Technical Paper, 2012.
[14] **Becher M., Becker S.** Investigation of the applicability of numerical noise prediction of an axial vehicle cooling fan. SAE Technical Paper, 2014.
[15] **Zanon A., De Gennaro M., Kuehnelt H., Caridi D., et al.** Numerical investigation of location and coherence of broadband noise sources for a low speed axial HVAC fan. SAE Technical Paper, 2014.
[16] **Pope Stephen B.** Turbulent Flows. Cambridge University Press, 2000.
[17] **Lowson M. V.** The sound field for singularities in motion. Proceedings of the Royal Society of London, Vol. 286A, 1965, p. 559-572.

Maotao Zhu received his B.S., M.S. and Ph.D. degrees in Vehicle Engineering from Jiangsu University, China, in 1985, 1990 and 2002, respectively. Now he is a Professor and the Director of Department of Vehicle Engineering, School of Automotive and Traffic Engineering, Jiangsu University, China. He is a member of the Society of Automotive Engineers of China. His research interests include automotive body engineering, modern design and test technology of automotive components.

Kuan Wang received his B.S. degree in Vehicle Engineering from Jiangsu University, China, in 2012. Now he is a postgraduate student, major in Vehicle Engineering, in School of Automotive and Traffic Engineering, Jiangsu University, China. His current research interests include computational fluid dynamics and computational aero acoustics methods and experimental methods in modern design of automotive components.

Pengfei Zhang received his B.S. degree in Vehicle Engineering from Jiangsu University, China, in 2013. Now he is a postgraduate student, major in Vehicle Engineering, in School of Automotive and Traffic Engineering, Jiangsu University, China. Presently he is particularly interested in computer aided design, computer aided engineering of automotive components.

Zhijun Li received his B.S. degree in Mechanical Engineering from Jiangsu Science and Technology University, China, in 2004. He received his M.S. degree in Vehicle Engineering from Jiangsu University, China, in 2013. Now he works at Jiangsu Chaoli Electric Co., Ltd., China, as a Project Manager and Design Director. His current research interest is low-noise high-performance automotive front-end cooling module design using numerical and experimental methods.